Stem Cell Reports
Article
ISSCR
OPEN ACCESS

FOXG1 dose tunes cell proliferation dynamics in human forebrain progenitor cells

Nuwan C. Hettige,[1,2] Huashan Peng,[2] Hanrong Wu,[2] Xin Zhang,[2] Volodymyr Yerko,[3] Ying Zhang,[2] Malvin Jefri,[2,7] Vincent Soubannier,[4,5] Gilles Maussion,[4,5] Shaima Alsuwaidi,[1,2] Anjie Ni,[1,2] Cecilia Rocha,[5] Jeyashree Krishnan,[6] Vincent McCarty,[1,2] Lilit Antonyan,[1,2] Andreas Schuppert,[6] Gustavo Turecki,[1,3,7] Edward A. Fon,[4] Thomas M. Durcan,[4,5] and Carl Ernst[1,2,3,7,*]

[1]Department of Human Genetics, McGill University, Montreal, QC H3A 0C7, Canada
[2]Psychiatric Genetics Group, Douglas Mental Health University Institute, 6875 Boulevard LaSalle, Montreal, QC H4H 1R3, Canada
[3]Department of Psychiatry, McGill University, Montreal, QC H3A 1A1, Canada
[4]McGill Parkinson Program and Neurodegenerative Diseases Group, Montreal Neurological Institute, Department of Neurology and Neurosurgery, Montreal, QC H3A 2B4, Canada
[5]The Neuro's Early Drug Discovery Unit (EDDU), McGill University, 3801 University Street, Montreal, QC H3A 2B4, Canada
[6]Institute for Computational Biomedicine, Aachen University, Pauwelsstraße 19, 52074 Aachen, Germany
[7]Integrated Program in Neuroscience, McGill University, Montreal, QC H3A 2B4, Canada
*Correspondence: carl.ernst@mcgill.ca
https://doi.org/10.1016/j.stemcr.2022.01.010

SUMMARY

Heterozygous loss-of-function mutations in Forkhead box G1 (*FOXG1*), a uniquely brain-expressed gene, cause microcephaly, seizures, and severe intellectual disability, whereas increased *FOXG1* expression is frequently observed in glioblastoma. To investigate the role of *FOXG1* in forebrain cell proliferation, we modeled *FOXG1* syndrome using cells from three clinically diagnosed cases with two sex-matched healthy parents and one unrelated sex-matched control. Cells with heterozygous *FOXG1* loss showed significant reduction in cell proliferation, increased ratio of cells in G0/G1 stage of the cell cycle, and increased frequency of primary cilia. Engineered loss of *FOXG1* recapitulated this effect, while isogenic repair of a patient mutation reverted output markers to wild type. An engineered inducible *FOXG1* cell line derived from a *FOXG1* syndrome case demonstrated that *FOXG1* dose-dependently affects all cell proliferation outputs measured. These findings provide strong support for the critical importance of *FOXG1* levels in controlling human brain cell growth in health and disease.

INTRODUCTION

The mammalian brain is a remarkable organ that must undergo several steps in development to ensure proper formation of specific brain structures. One unique structure of the brain is called the cerebral cortex, and it is derived from neural progenitor cells (NPCs) (Foley et al., 2000; Nieuwkoop, 1947; Rakic, 2006). NPCs proliferate to a precise number, differentiate, and migrate to become cerebral cortical cells. Cellular expansion prior to cell differentiation is tightly regulated (Caviness et al., 1995; Rakic and Caviness, 1995), but how NPCs know when to stop proliferating and begin differentiating is not well understood. This remains a fundamental question despite extensive work to reveal important parts of this pathway (Egger et al., 2011; Homem et al., 2015). The factors that control when NPCs proliferate or differentiate (Ernst, 2016) are fundamental to understanding many neurodevelopmental diseases in humans.

Microcephaly is a disorder of development affecting about 7 in 10,000 live births (Hanzlik and Gigante, 2017). It is defined as a head circumference less than 2 standard deviations below the mean for gender and age and can be present from birth (termed "primary" microcephaly) or post-natally. Glioblastoma multiforme (GBM) is a severe form of brain tumor that has a median survival of 15 months from diagnosis and an incidence rate of 3 per 100,000 people per year (Cloughesy et al., 2014). A core feature of both primary microcephaly and GBM is that they likely depend on the activity of NPCs. NPCs must expand significantly as the brain develops to form the appropriate number of cells, whereas too little expansion can lead to primary microcephaly. In GBM, hallmark genes of NPCs are reactivated to drive tumor cell growth (Lathia et al., 2015). An understanding of the critical regulators of NPC proliferation is thus essential for understanding both primary microcephaly and GBM.

FOXG1 is a member of the FOX superfamily, characterized by the amino acid forkhead domain, that associates with DNA to affect neurodevelopmental programming (Golson and Kaestner, 2016). It is uniquely brain expressed (Murphy et al., 1994) and there is significant evidence supporting the role of *FOXG1* in expanding the NPC pool from human and mouse studies. Human *FOXG1* syndrome (OMIM: 164874), in which one copy of *FOXG1* is mutated, leading to loss of function, is a recognized microcephaly syndrome (Ariani et al., 2008). *Foxg1* knockout in mice leads to an absent or extremely stunted telencephalon

(Hanashima et al., 2004; Xuan et al., 1995). Without *Foxg1* or with reduced dosage, NPCs prematurely exit the cell cycle, as evidenced by an increased frequency of cells in G1/G0 phase (Hanashima et al., 2002, 2004; Xuan et al., 1995). In humans, overexpression of *FOXG1* is observed in glioblastoma (Chen et al., 2018; Seoane et al., 2004) and promotes brain tumor growth (Verginelli et al., 2013). These data provide clinically relevant evidence that *FOXG1* dosage has a severe impact on NPC proliferation (Hettige and Ernst, 2019).

Recent advances in stem cell biology have allowed for *in vitro* human modeling of cortical brain development, preserving major developmental milestones (Ardhanareeswaran et al., 2017). Stem cells derived from a somatic cell (Takahashi et al., 2007) are differentiated to ectoderm and then neuralized using factors known to be present at critical time points in neurodevelopment (Bell et al., 2019). The temporal sequence of NPC proliferation and differentiation is determined by the sequential activation of growth factors and other small molecules (Kohwi and Doe, 2013) provided by the experimenter. Thus, important mechanisms such as those involved in the switch from proliferation to differentiation of NPCs can be studied in cells that meet defining characteristics of a cell type, such as expression of markers or physiological properties of the cell.

To date, a handful of studies have used induced pluripotent stem cells (iPSCs) to model *FOXG1* syndrome. In 2016, Patriarchi et al. generated iPSC-derived neurons from two *FOXG1*$^{+/-}$ cases and observed an imbalance in excitatory/inhibitory synaptic protein expression (Patriarchi et al., 2016). However, these data did not explore the dynamics of *FOXG1* dose as NPCs develop. To investigate *FOXG1* dose, Zhu et al. (2019) used a tunable degron motif to modify the expression of endogenous *FOXG1*, and they observed an increased G1 phase of NPCs and increased proportion of GABAergic interneurons after NPC differentiation (Zhu et al., 2019). What is currently missing is a comprehensive, robust investigation of the role of *FOXG1* mutations that cause microcephaly. Here, we use human patient cells and engineered lines to assess how changes in *FOXG1* dose might lead to cellular phenotypes relevant to disease.

RESULTS

Identifying the timing of *FOXG1* expression in developing neurons

In rodent neurodevelopment, *Foxg1* is expressed at E8.5 (Tao and Lai, 1992), but the point at which *FOXG1* is turned on for human *in vitro* differentiation protocols remains unknown. To examine the dynamics of *FOXG1* expression in human neurodevelopment, we reprogrammed somatic cells into pure iPSC colonies while simultaneously inserting a tdTomato tag onto endogenous *FOXG1* (Bell et al., 2019). iPSCs were induced to become NPCs over a 12-day differentiation period after which cells were suspended and purified for 2–3 days for NPC purification (Figure 1A). To ensure the successful differentiation of NPCs, iPSC lines underwent extensive quality-control screening, including copy-number variation (CNV) analysis and endogenous-marker staining (Figure 1B). We define NPCs as intermediate forebrain progenitors that express specific neural stem cell markers (Figure 1C) and proliferate in maintenance medium with the potential to differentiate into forebrain neurons. Forebrain cortical neurons are defined by their morphology and expression of the neuronal markers MAP2 and TUJ1 (Figure 1D). Using a purified iPSC line that successfully integrated the tdTomato tag to endogenous *FOXG1* (Figure 1E), we live imaged cells over the 12-day NPC induction period and for 6 days post-differentiation in NPC maintenance medium without mechanical purification. This allowed us to assess direct effects of culture conditions and compare across time points (i.e., without passaging cells). Beginning at day 5, we observed the presence of a red signal in some differentiating iPSC colonies. A higher proportion of cells became noticeably red at day 7 (Figure 1F), coinciding with the fact that we could detect neural stem cell markers, NESTIN and SOX1, at this same time point (Figure 1G). As the colonies continued to differentiate into NPCs, we observed that the majority of the cells displayed a red signal by approximately day 12. After 12 days in neural induction medium, cells were switched to NPC maintenance medium. Notably, the longer NPCs were kept in maintenance medium, the fainter the red signal became (Figure 1F). This live-cell reporter assay suggests that *FOXG1* is induced relatively early in the stem cell neural-induction process and that it is likely at peak expression here due to exposure to factors in the induction medium. *FOXG1* levels are substantial but decrease the longer cells are maintained and passaged in maintenance medium. To confirm our findings from the cell reporter assay, we validated results using three independent and healthy stem cell lines to confirm FOXG1 changes during neural induction. After first ensuring that the antibody could detect FOXG1 (Figure S1), we detected FOXG1 as early as day 7 during neural induction. While there is cell-line variability, FOXG1 is nevertheless expressed at relatively early stages during neural induction (Figure 1H).

Previous reports on *Foxg1* in mice have suggested a continued role in differentiated neural cells (Cargnin et al., 2018; Dastidar et al., 2011); therefore, we next wondered about *FOXG1* expression during *in vitro* forebrain neuron differentiation from human NPCs. We began with the reporter assay for neural differentiation but

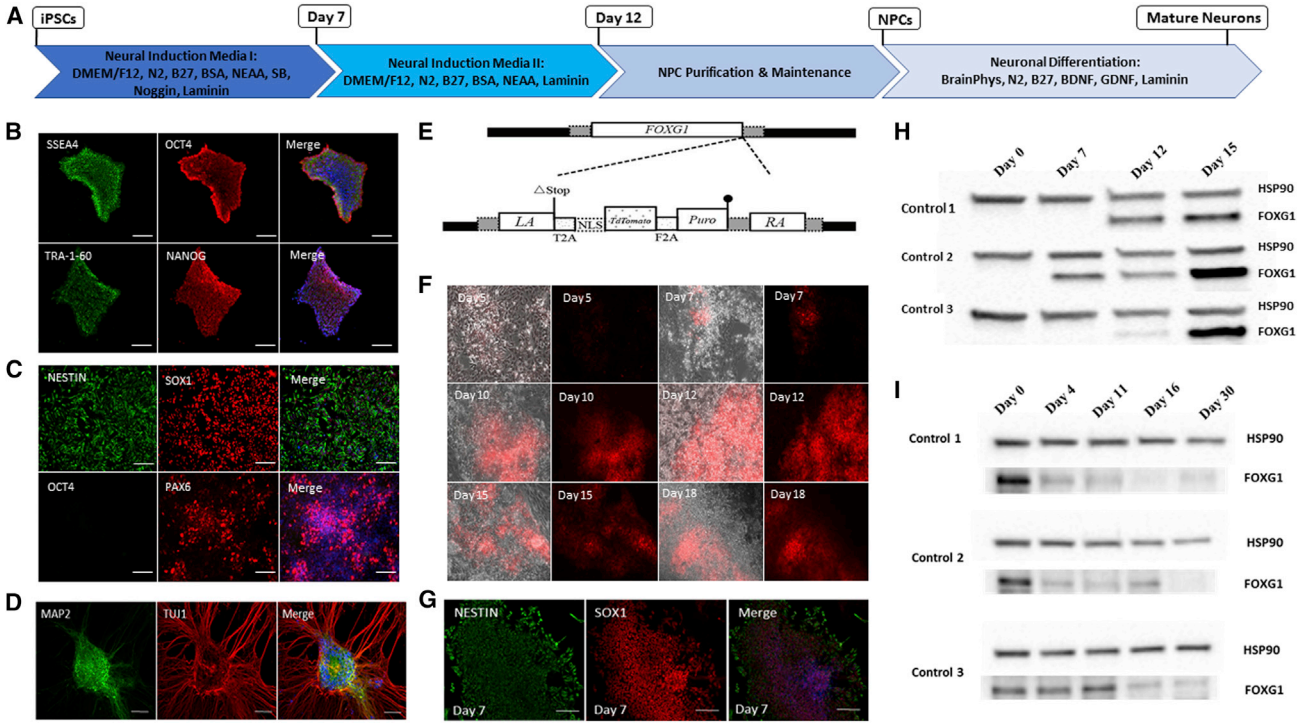

Figure 1. Tracking *FOXG1* expression across forebrain neural progenitor induction and neuronal differentiation

(A) Schematic diagram of procedure to generate iPSC-derived forebrain neural progenitor cells and neurons.

(B) Representative immunofluorescence images of iPSCs stained for standard markers of pluripotency. Scale bar, 50 μm.

(C) Representative immunofluorescence images of NPCs stained for standard forebrain neural progenitor markers and the pluripotency marker, OCT4. Scale bar, 50 μm.

(D) Representative immunofluorescence images of cortical forebrain neurons stained for MAP2 (green) and TUJ1 (red). Scale bar, 50 μm.

(E) Schematic diagram of *FOXG1*-reporter construct transfected into a control line. This construct contains a TdTomato (tandem dimer Tomato), which is an exceptionally bright red fluorescent protein that allows for visualization of *FOXG1* in live cells. The components of the construct are as follows: RA, right arm; LA, left arm; NLS, nuclear localization signal; T2A and F2A, two types of 2A signaling to enable translational gapping between two proteins; Stop, stop codon; Puro, puromycin resistance gene.

(F) Representative images of *FOXG1*-reporter iPSCs differentiated toward neural progenitor cells. Red signal indicates expression of *FOXG1*.

(G) Immunofluorescence images of cells at day 7 of neural induction expressing markers of NPC identity, NESTIN and SOX1. Scale bar represents 50 μm.

(H) Western blot of FOXG1 in control iPSCs over multiple time points during neural induction to NPCs.

(I) Western blot of FOXG1 in control NPCs over multiple time points during differentiation into cortical neurons.

observed continuous and sustained signal (not shown). Since we could not rule out that the red signal was being maintained due to a lack of tdTomato degradation rather than sustained *FOXG1* expression, we reasoned that directly measuring protein expression in three healthy lines would be more interpretable. We observed a decrease in *FOXG1* expression as NPCs differentiated into neurons until day 30 (Figure 1I). While *FOXG1* expression decreases throughout neural differentiation, it is detectable at low levels at later time points, which may be a dose that suffices to perform previously reported actions of *FOXG1* in post-mitotic neurons (Cargnin et al., 2018). That said, these experiments demonstrate that *FOXG1* expression peaks during neural induction (possibly due to exposure to the "dual SMAD" inhibitors SB431542 and Noggin; Chambers et al., 2009), decreases during continued proliferation in an NPC maintenance medium, and decreases further during neuronal differentiation.

Generation and characterization of *FOXG1* syndrome-derived cells

We generated iPSCs and NPCs from three clinically diagnosed *FOXG1* syndrome cases, all of whom had microcephaly (Figure 2A). Two of three cases were matched to their own biological mothers, while the third case was age and sex matched to an unrelated female. We derived iPSCs from fibroblasts or urine renal epithelial cells and confirmed expression of pluripotent markers (Figure S2).

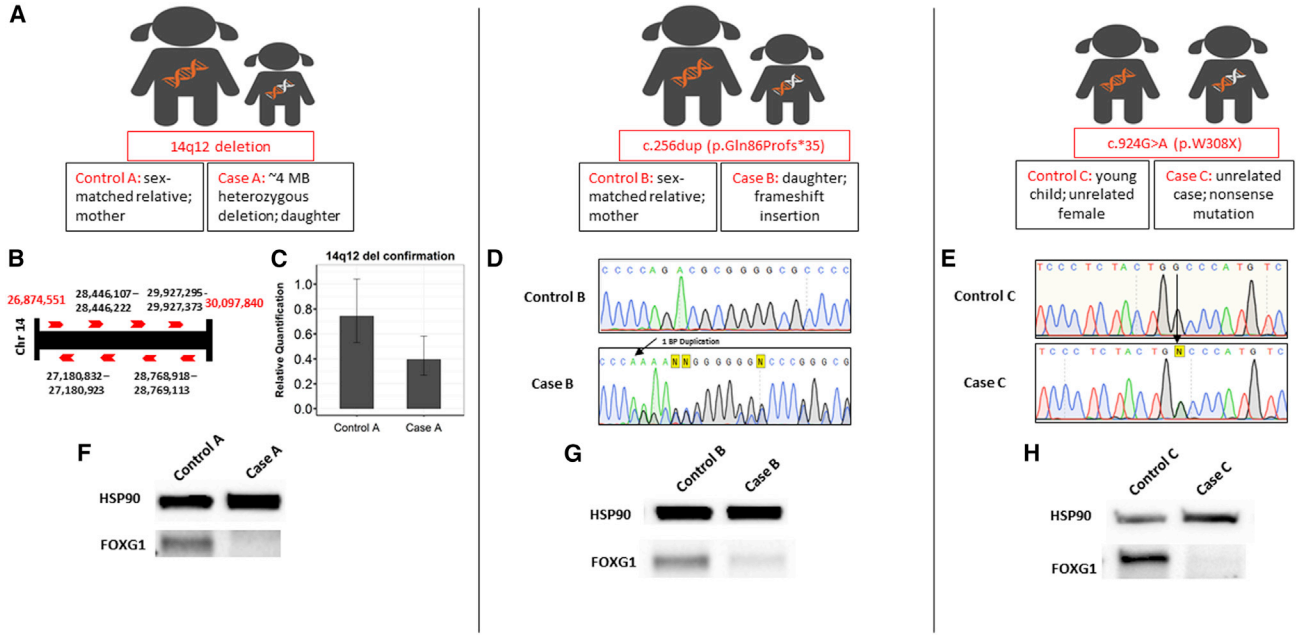

Figure 2. iPSC-derived models of *FOXG1* syndrome

(A) Illustrative diagram of *FOXG1* syndrome cases, their genetic mutations, and matched controls.

(B) Illustrative diagram indicating genomic coordinates of case A 14q12 deletion and primers used to validate deletion using qPCR of genomic DNA.

(C) qPCR validation of case A 14q12 deletion indicating decreased presence of 14q12 DNA. Error bars denote SEM.

(D) Sanger sequencing of case B and healthy control B at the site of reported *FOXG1* mutation.

(E) Sanger sequencing of case C and healthy control C at the site of reported *FOXG1* mutation.

(F) Western blot of control and case A NPCs demonstrating reduced FOXG1 dosage.

(G) Western blot of control and case B NPCs demonstrating reduced FOXG1 dosage.

(H) Western blot of control and case C NPCs demonstrating reduced FOXG1 dosage.

We confirmed reported mutations in DNA (Figures 2B–2E, Table S1) and then derived forebrain NPCs for the six lines and confirmed expression of NPC markers (Figure S2). We were able to successfully induce NPCs from all cell lines, suggesting that the heterozygous loss of *FOXG1* does not interfere with neural induction. FOXG1 protein levels were assessed via western blot from all cases and controls. Because case A has a complete gene deletion, case B has a frameshift, and case C has a premature stop codon, we expected and found decreased FOXG1 protein in all cases (Figures 2F–2H).

Pathogenic mutations in *FOXG1* affect cell proliferation in human forebrain progenitor cells

Rodent loss-of-function studies have suggested that *Foxg1* affects neural progenitor cell expansion, possibly implying a role in the regulation of NPC proliferation. Our initial observation of cultured case/control NPCs was that there was a reduction in proliferation in disease cells (Figure S3A). To formally assess this hypothesis, we performed a bromodeoxyuridine (BrdU) pulse-chase experiment. First, we piloted the length of the BrdU pulse in one case/control pair and found saturation of BrdU after 24 h (Figure S3B), suggesting that cells are highly proliferative, irrespective of genotype. We were able to see non-saturation at 4 h of BrdU treatment and so selected this time point for formal study. Across all three cases, we observed a marked reduction in BrdU fluorescence compared with control NPCs (Figures 3A and 3B), suggesting that the heterozygous loss of *FOXG1* is associated with less BrdU incorporation, which can be interpreted as a proxy for cell proliferation. This might suggest delayed cell proliferation and could explain the lower number of cells in *FOXG1*-mutation NPCs. If this were true, we might expect changes in the proportion of cells in a given phase of the cell cycle. Briefly, DNA content can be used as a proxy for cell-cycle phase as the G0/G1 growth phase has half as much DNA as the G2/mitosis phase, whereas the synthesis (S) phase has intermediate levels. Cells with altered proliferation rates may show changes in the proportion of cells within each phase. With *FOXG1* loss, we might expect an increased proportion of cells in G0/G1, which could reflect a slowing or

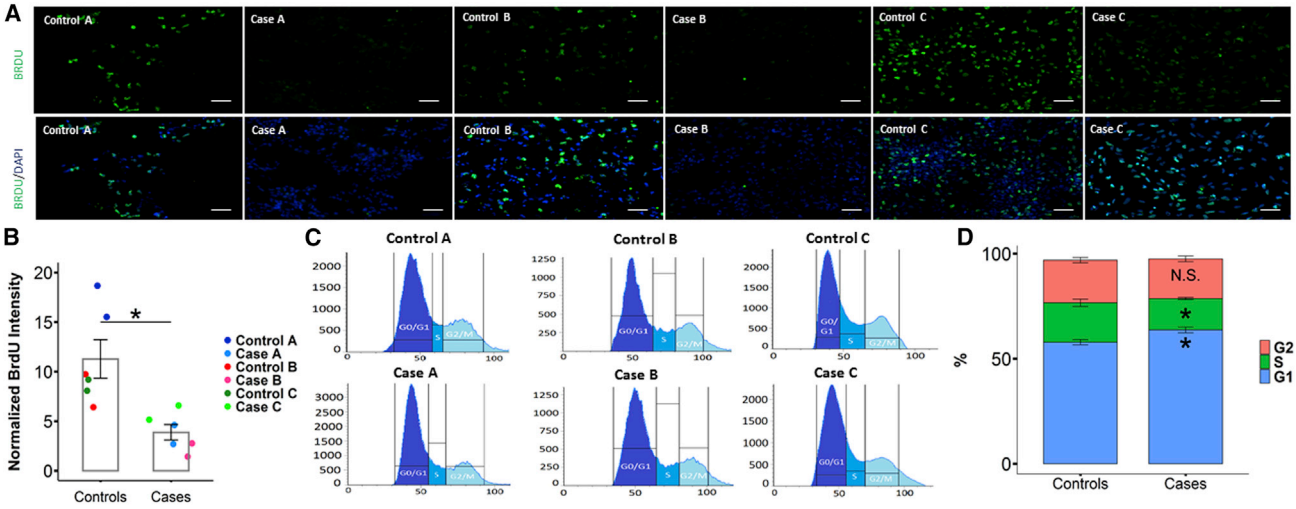

Figure 3. Evidence for reduced proliferative capacity in forebrain neural progenitor cells from *FOXG1* syndrome cases

(A) Representative images of BrdU staining in NPCs from three cases and three controls after 4 h of BrdU incubation. Scale bar, 50 μm.

(B) Measurement of normalized BrdU fluorescence intensity across pooled cases and controls (n = 3 controls and 3 cases; two images each from two independent replicates quantified per line for a total of 12 experiments). Error bars denote SEM. Significance is based on Student's t test (*p < 0.05).

(C) Histogram of case and matched control NPCs stained with Hoechst 33342 DNA dye showing DNA content distribution. G0/G1 and G2/M peaks are separated by the S phase distribution.

(D) Stacked-bar plots illustrating the ratio of NPCs in case and matched control NPCs sorted as being in G1/S/G2 phases of the cell cycle (n = 3 controls and 3 cases; four independent FACS runs quantified per condition for a total of 24 FACS experiments). Error bars denote SEM. Statistical comparisons are made for each cell-cycle phase. Significance is based on Student's t test (*p < 0.05).

premature exit from the cell cycle. To test this, we fixed and stained equal numbers of proliferating NPCs with the DNA dye Hoechst 33342 and then sorted NPCs according to a standard fluorescence-activated cell-sorting (FACS) protocol for cell-cycle analysis. We ran three separate experiments for all case and control cell lines for a total of 18 cell sorts and found a consistent increase of cells in G0/G1 at the expense of cells in G2 phase (Figures 3C and 3D). Irrespective of how the data were analyzed or how phases were systematically delineated (not shown), the result was consistent. We interpret these data to mean that loss of *FOXG1* either increases the length of time in G0/G1 or results in a faster exit from G2 phase.

Heterozygous loss-of-function *FOXG1* mutations recapitulate cell proliferation deficits observed in *FOXG1* syndrome NPCs

Our sample size of three *FOXG1* syndrome cases with two familial and one unrelated control was sufficient to detect cell proliferation effects; however, we wanted to assess these outputs in a more controlled way, albeit one that it is not directly related to the syndrome itself. We reasoned that creating heterozygous knockout (KO) cells and comparing these to isogenic controls should recapitulate findings from patient cells and allow us to state more conclusively that this phenomenon is caused by heterozygous *FOXG1* loss, because genetic background and *FOXG1* mutation type were no longer potential sources of variation. To do this, we used our simultaneous reprogramming and gene-editing protocol (Bell et al., 2017) to generate clonal loss-of-function (LOF) *FOXG1* models in an independent control line (control D) (Figure S4A). We designed guide RNAs (gRNAs) to target the intergenic region of *FOXG1* (Figure S4B) to induce a frameshift mutation, leaving one functional copy of *FOXG1*. We expanded six iPSC clones and selected two reprogrammed iPSC lines suspected to be gene edited based on band shift patterns observed using gel electrophoresis where two bands were present (Figure S4C). Sanger sequencing of both alleles (wild type and edited) confirmed that iPSC colonies 1 and 2 both had a heterozygous 40-bp deletion that differed by 7 bp (Figure 4A). Both lines were consistent for all iPSC markers (Figure S2). After differentiating control D and two isogenic LOF models (hereafter labeled LOF-KO1 and LOF-KO2) into NPCs (Figure S2), we assessed FOXG1 protein levels, which were significantly reduced (Figure 4B). A detailed description of all control and LOF lines can be found in Table S1.

Using these LOF models, we performed the same bright-field, BrdU, and FACS proliferation assays as on our *FOXG1* syndrome cases. Day 0 and day 1 bright-field images showed a marked reduction in the number of NPCs in

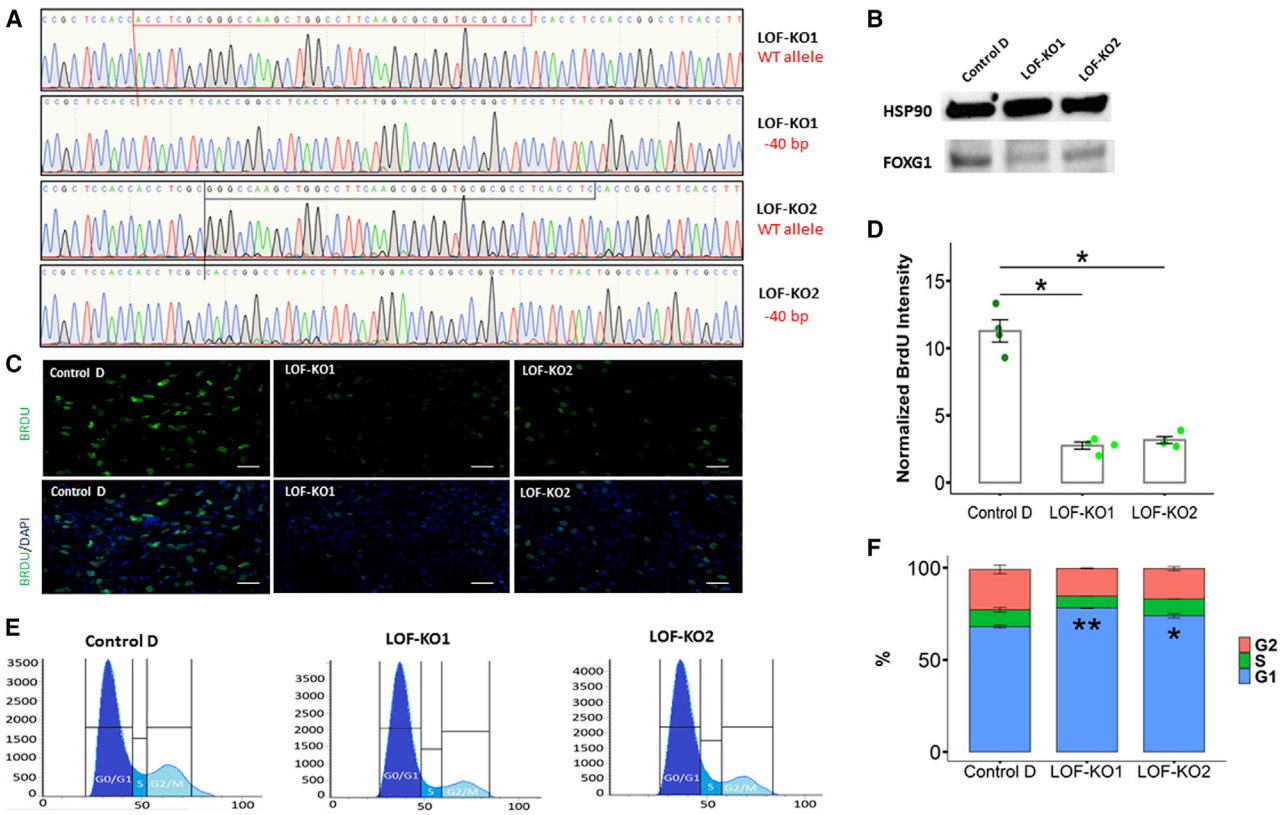

Figure 4. Forebrain neural progenitor cells from heterozygous loss-of-function *FOXG1* models recapitulate delayed cell division

(A) Sanger sequencing of the wild-type and edited alleles for LOF-KO1 and LOF-KO2 at the site of reported *FOXG1* deletion. Sequencing reveals heterozygous 40-bp deletions (different sites) in both lines.

(B) Western blot of control D compared with LOF-KO1 and LOF-KO2 NPCs demonstrating reduced FOXG1 protein.

(C) Representative images of BrdU staining in NPCs from control D, LOF-KO1, and LOF-KO2 after 4 h of BrdU incubation. Scale bar, 50 μm.

(D) Measurement of normalized BrdU fluorescence intensity across control D, LOF-KO1, and LOF-KO2 (n = 1 control and 2 KOs; 4 images from 2 independent replicates quantified per line for a total of 12 experiments). Error bars denote SEM. Significance is based on Student's t test (*$p < 0.05$).

(E) Histograms of control D, LOF-KO1, and LOF-KO2 NPCs stained with Hoechst 33342 DNA dye showing DNA content distribution. G0/G1 and G2/M peaks are separated by the S-phase distribution.

(F) Stacked-bar plots illustrating the ratio of NPCs in LOF-KO1 and LOF-KO2 compared with isogenic control D NPCs sorted as being in G1/S/G2 phases of the cell cycle (n = 1 control and 2 KOs; two independent replicates quantified per line for a total of 12 FACS experiments). Error bars denote SEM. Statistical comparisons are made for each cell-cycle phase. Significance is based on Student's t test (*$p < 0.05$; **$p < 0.005$).

LOF-KO1 and LOF-KO2 after 24 h of proliferation (Figure S3A). BrdU staining and FACS assays of NPCs also demonstrated results similar to those of *FOXG1* syndrome cases (Figures 4C–4F).

Increased number of primary cilia associated with decreased *FOXG1* in cases and in engineered heterozygous KOs

Primary cilia are sensory organelles dynamically regulated during cell-cycle progression (Pugacheva et al., 2007). Formation of cilia typically begins at the G0/G1 phase, while disassembly occurs as cells enter S phase (Figure 5A) (Sanchez and Dynlacht, 2016). We reasoned that the impaired cell-cycle dynamics identified in human *FOXG1*-deficient NPCs might also affect the observed frequency of cilia. We first developed our assay for ARL13B, a commonly used marker of primary cilia, by optimizing staining and performing confocal microscopy to ensure staining patterns matched expectations of cilia position (Figures 5B and 5C). Following careful calibration of our assay, we stained case and control NPCs and quantified the number of cilia per nucleus across multiple images. We identified a significant increase in the number of ARL13B-positive cilia in all *FOXG1* syndrome cases compared with their

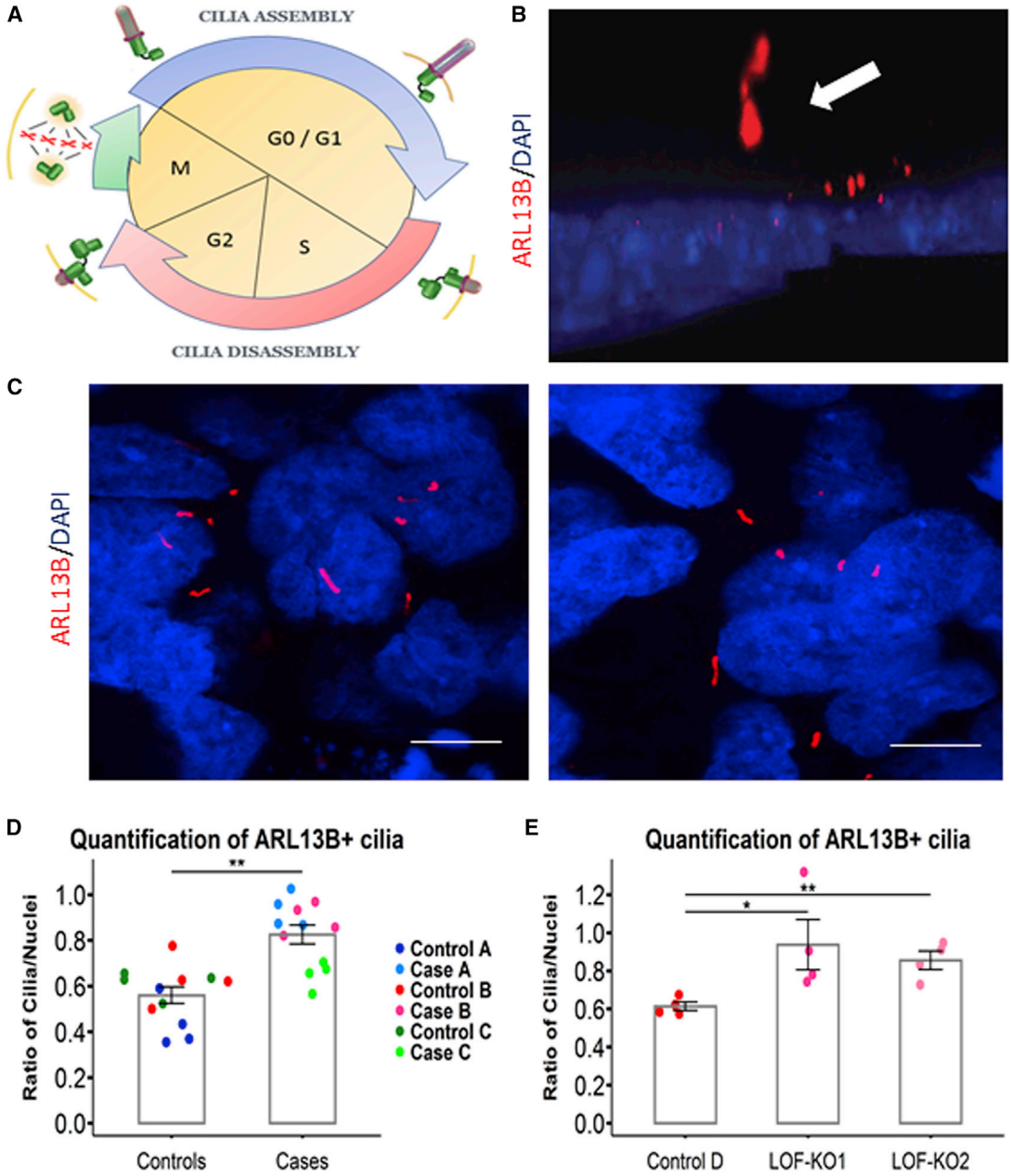

Figure 5. Loss of *FOXG1* leads to increased primary cilia in forebrain neural progenitor cells

(A) Illustrative diagram depicting the assembly of primary cilia in coordination with the phases of the cell cycle.

(B) Stacked 3D immunofluorescence image of ARL13B^{+} primary cilia in NPCs with nuclei stained with DAPI. White arrow points to an example of a cilium visualized in high resolution with its distinct elongated structure.

(C) Representative immunofluorescence of ARL13B to visualize primary cilia in forebrain NPCs. Scale bar, 25 μm.

(D) Quantification of ARL13B^{+} primary cilia in all cases versus matched controls (n = 3 controls and 3 cases; four images from four independent replicates quantified per line for a total of 24 experiments). Error bars denote SEM. Significance is based on Student's t test (**p < 0.005).

(E) Quantification of ARL13B^{+} primary cilia shown in KOs and isogenic control NPCs (n = 1 control and 2 KOs; four images from four independent replicates quantified per line for a total of 12 experiments). Error bars denote SEM. Significance is based on Student's t test (*p < 0.05; **p < 0.005).

matched control NPCs (+47% increase, SE = 0.0597, p = 0.0071) (Figure 5D). Similarly, we stained and quantified cilia in LOF models to find more cilia in LOF-KO1 (+53% increase, SE = 0.0886, p = 0.0521) and LOF-KO2 (+39% increase, SE = 0.0469, p = 0.0041) compared with isogenic control D (Figure 5E).

Cortical spheroids show decreased size, and organoids show premature neuronal differentiation, in *FOXG1* mutant cases

To further support our argument of decreased cell proliferation with reduced FOXG1 dosage, we modeled two *FOXG1* cases (cases A and B) with their sex-matched familial controls (controls A and B) using 3D spheroid cultures. By utilizing the hanging-drop method, an equal number of cortical NPCs were allowed to form spheroids in suspension culture with regular maintenance medium. Bright-field images were taken after spheroids had formed (day 0) and 7 days after spheroids were allowed to proliferate (day 7) (Figure S5A). By quantifying the area of the spheroids, we first confirmed there was no significant difference in size at day 0 (SE = 0.7541, p = 0.1513). However, we observed, on average, smaller spheroid sizes in cases compared with matched controls at day 7 (+31% smaller, SE = 5.3437, p = 0.0259) (Figure S5B).

Given that previous reports suggested that *Foxg1* functions to suppress neuronal differentiation in mice (Hanashima et al., 2002, 2004; Xuan et al., 1995), we aimed to assess whether this was also true in humans with *FOXG1* syndrome who had familial sex-matched controls. By differentiating NPCs to neurons in 2D cultures, we first qualitatively observed what appeared to be increased frequency of processes and polarization of NPCs, indicative of early neuronal differentiation (Figure S6A). To assess premature differentiation more quantitatively in cortical organoids, we differentiated NPCs to organoids for the same two cases (cases A and B) and matched controls (controls A and B) using the hanging-drop method and switching to neuronal differentiation medium. At 15 days post-differentiation, we fixed and sectioned organoids to stain for NPC markers, NESTIN and SOX1, and neuronal markers, MAP2 and TUJ1 (Figure S6B). In cases, we observed decreased signal for NESTIN (SE = 0.0571, p = 0.0083) and SOX1 (SE = 0.0461, p = 0.0084) and increased signal for MAP2 (SE = 0.0329, p = 0.0069) and TUJ1 (SE = 0.0297, p = 0.0034) (Figure S6C). We interpreted this as supportive evidence for *FOXG1* syndrome organoids undergoing earlier neuronal differentiation. As the expression of NPC markers was decreased (lower fluorescence) and expression of neuronal markers was increased (higher fluorescence), this was suggestive that *FOXG1* syndrome organoids adopted a more neuronal cellular identity quicker than control organoids.

Genetic repair of mutant *FOXG1* reverses cell proliferation phenotypes

To demonstrate unequivocally that cellular proliferation phenotypes were due solely to a mutation in *FOXG1*, we used cells from case C, who had no matched familial control, to reverse cell proliferation phenotypes. We performed simultaneous homology-directed repair gene editing with stem cell reprogramming. This technique does not guarantee clonality but has very high purity of selected populations (Bell et al., 2017). We expanded nine clones and confirmed successful editing in two potential lines via Sanger sequencing (Figure 6A). We estimate our repair efficiency to be about 70%–80% based on Sanger-sequencing traces and performed all experiments with cell passage 1 or 2. We differentiated one iPSC repair line and the unedited case C iPSC line into NPCs (Figure S2) and quantified the level of FOXG1 protein. We found significantly increased FOXG1 expression in the repair NPC line, confirming that we had successfully restored FOXG1 dosage (Figure 6B). Next, we assessed whether cell proliferation outputs and cilia number in repair NPCs had also been altered toward a more control-like state. We observed a significantly increased rate of proliferation according to the BrdU assay (Figure 6C) and a significantly reduced proportion of NPCs delayed at G0/G1 of the cell cycle in repair NPCs (Figures 6D and 6E). We also observed a significant reduction in the number of ARL13B-stained primary cilia compared with case C (Figure 6F). These results suggest that the nonsense mutation in *FOXG1* in case C was directly responsible for the cell-proliferation effects observed.

FOXG1 deficiency does not increase apoptosis

We also assessed cell death in NPC cultures across different *FOXG1*-deficiency models. Using a terminal deoxynucleotidyl transferase dUTP nick-end labeling (TUNEL) assay to stain and image cells undergoing apoptosis, we compared the number of apoptotic cells between $FOXG1^{+/-}$ models and their matched controls (Figure S7A). We observed no significant difference in cell death (Figure S7B), concluding that it is the rate of NPC proliferation that is correlated with *FOXG1* dose.

FOXG1 dose-dependently affects cell proliferation

To determine if *FOXG1* dose affects cell proliferation outputs, we engineered an inducible *FOXG1* construct using a TET-On promoter to tune *FOXG1* levels in case B cells. Using a gRNA targeting the *AAVS1* locus, we inserted a doxycycline-inducible *FOXG1* construct containing a cleavable red fluorescent protein (RFP) reporter (Szymczak and Vignali, 2005) and a non-cleavable tandem affinity purification (TAP) tag into NPCs (Figure 7A). We used PCR and Sanger sequencing to confirm the insertion from five iPSC clones and then selected a successfully integrated

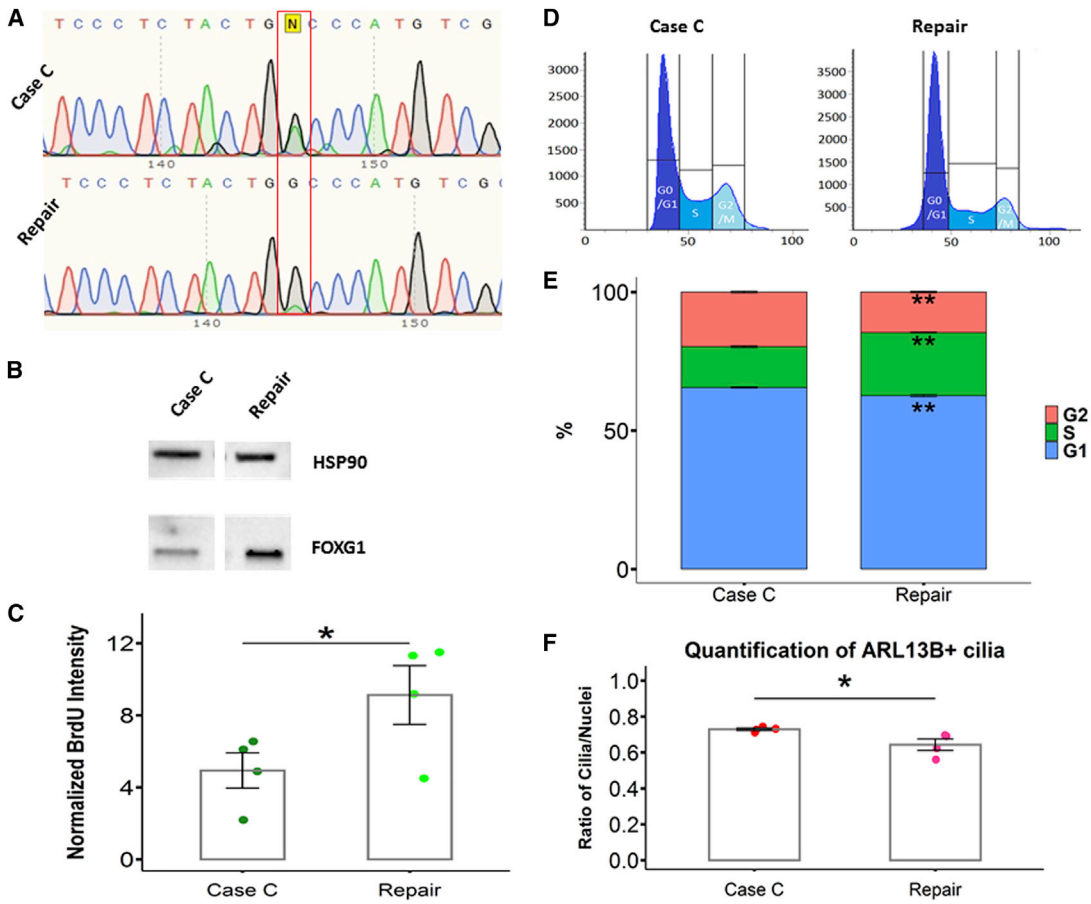

Figure 6. Genetically engineered repair of endogenous mutant *FOXG1* from case C rescues output markers of proliferative capacity in forebrain neural progenitor cells

(A) Sanger sequencing of case C and isogenic *FOXG1* repair at the site of reported *FOXG1* mutation (c.924G>A).

(B) Western blot of FOXG1 expression in case C and repair NPCs demonstrating the restoration of wild-type FOXG1 levels in the repair line. Lanes are cut to show only case C NPCs and the successful repair NPCs with significantly increased FOXG1 expression.

(C) Measurement of normalized BrdU fluorescence intensity in case C compared with repair (n = 1 case C and 1 repair; two images from two independent replicates quantified per line for a total of four experiments). Error bars denote SEM. Significance is based on Student's t test (*$p < 0.05$).

(D) FACS histogram delineating segregation of cells according to cell-cycle phase (G0/G1, S, or G2/M).

(E) Stacked-bar plots illustrating the ratio of case C to repair NPCs sorted as being in G1/S/G2 phases of the cell cycle (n = 1 case C and 1 repair; four independent replicates quantified per line for a total of eight FACS experiments). Error bars denote SEM. Statistical comparisons are made for each cell-cycle phase. Significance is based on Student's t test (**$p < 0.005$).

(F) Quantification of ARL13B-positive primary cilia from NPCs shown in (D) (n = 1 case C and 1 repair; four images from four independent replicates quantified per line for a total of eight experiments). Error bars denote SEM. Significance is based on Student's t test (*$p < 0.05$).

line for neural induction (Figure S2). After induction and purification of NPCs, doxycycline was administered at titrated concentrations for 3 days, whereupon we extracted protein to determine if we could tune FOXG1 protein levels based on doxycycline concentrations (Figure 7B). We estimate increases in FOXG1 over the no-doxycycline condition to be 1.2-, 1.5-, and 2-fold at doxycycline concentrations of 0.125, 0.50, and 1.00 μg/μL, respectively. We also tested if there were dose-dependent effects of FOXG1 on cell proliferation output markers. As the concentration of doxycycline was increased, the number of NPCs labeling for BrdU increased (Figure 7C). Similarly, a dose-dependent negative correlation was observed between FOXG1 expression and proportion of cells in G0/G1 (Figure 7D) and frequency of primary cilia (Figure 7E). These data suggest that changing *FOXG1* dosage in cells derived from a person with *FOXG1* syndrome directly affects cell proliferation outputs and points to a very tight relationship between *FOXG1* dose and degree of NPC proliferation.

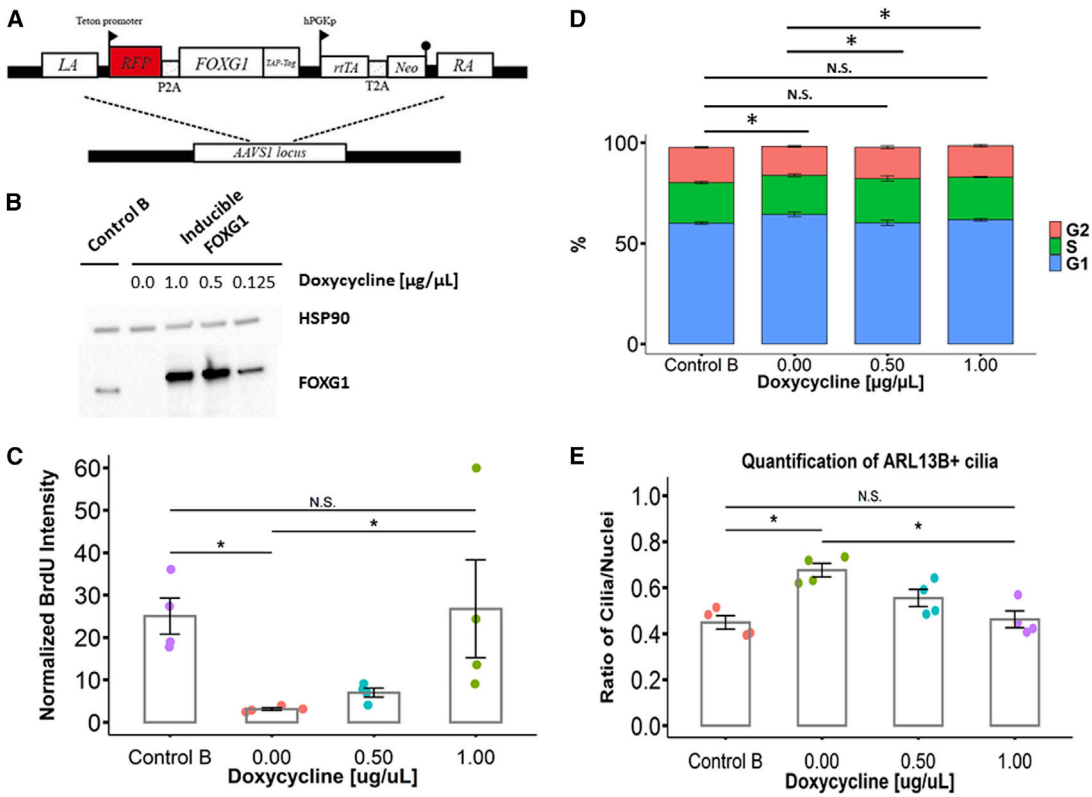

Figure 7. Inducible *FOXG1* expression reduces primary cilia and increases proliferation in case B neural progenitor cells.

(A) Illustrative diagram of the TET-On inducible vector integrated into the *AAVS1* locus of case B using CRISPR-Cas9 gene editing. The components of the construct are as follows: LA, left arm; RA, right arm; RFP, red fluorescent protein; P2A and T2A, two types of 2A signaling to enable translational gapping between two proteins; TAP-Tag, tandem affinity purification tag; hPGKp, human phosphoglycerate kinase promoter; rtTA, reverse tetracycline-controlled transactivator; Neo, Neomycin resistance gene.

(B) FOXG1 protein levels after treatment with titrated concentrations of doxycycline (0, 1, 0.5, and 0.125 μg/mL) in inducible-*FOXG1* NPCs compared with control B NPCs.

(C) Measurement of normalized BrdU fluorescence intensity across doxycycline concentrations (n = 1 control B, 1 inducible *FOXG1* with 0 μg/mL, 1 inducible *FOXG1* with 0.5 μg/mL, and 1 inducible *FOXG1* with 1 μg/mL doxycycline concentration; two images from two independent replicates quantified per line for a total of eight experiments). Error bars denote SEM. Significance is based on Student's t test (*p < 0.05; N.S., non-significant).

(D) Stacked-bar plots illustrating the ratio of NPCs in control B and inducible *FOXG1* sorted as being in G1/S/G2 phases of the cell cycle (n = 1 control B, 1 inducible *FOXG1* with 0 μg/mL, 1 inducible *FOXG1* with 0.5 μg/mL, and 1 inducible *FOXG1* with 1 μg/mL doxycycline concentration; four independent replicates quantified per line for a total of 16 FACS experiments). Error bars denote SEM. Statistical comparisons were made for each cell-cycle phase. Statistical comparisons were made between G0/G1 phases of the cell cycle (*p < 0.05; **p < 0.005; N.S., non-significant).

(E) Quantification of ARL13B-positive primary cilia from NPCs shown in (D) (n = 1 control B, 1 inducible *FOXG1* with 0 μg/mL, 1 inducible *FOXG1* with 0.5 μg/mL, and 1 inducible *FOXG1* with 1 μg/mL doxycycline concentration; four images from four independent replicates quantified per line for a total of 16 experiments). Error bars denote SEM (*p < 0.05; **p < 0.005; N.S., non-significant).

DISCUSSION

Alterations in *Foxg1* levels have long been known to affect cell proliferation across different non-human species (Li and Vogt, 1993). We have provided several lines of evidence in patient-derived human cells to suggest that disease-causing mutations leading to haploinsufficiency of *FOXG1* support this finding. Our data demonstrate that NPCs are a good developmental time point at which to assess *FOXG1* function because both functional copies of the gene do not appear to be required for neural induction from stem cells, major downstream patterning effects have not yet occurred, and NPCs are highly mitotically active.

We discovered that loss of *FOXG1* is consistent with increased frequency of primary cilia on NPCs, which has

not been reported in any previous models of *FOXG1* deficiency to our knowledge. This finding could either be consistent with increased time in G0/G1 phase of the cell cycle or implicate *FOXG1* in the regulation of cilia formation and disassembly. Ciliopathies are diseases where mutations occur in genes that encode proteins directly involved in cilia (Liu et al., 2021; Waters and Beales, 2011). They have a particular constellation of symptoms, many of which (in addition to microcephaly; Guemez-Gamboa et al., 2014) are inconsistent with *FOXG1* syndrome. We favor the model whereby the increased occurrence of primary cilia on NPCs is a result of the changes in cell cycle or proliferation , rather than *FOXG1* being a direct actor on cell ciliary dynamics.

How might *FOXG1* dose affect NPC expansion? The presence of the FOX domain suggests that *FOXG1* action is through DNA binding (Golson and Kaestner, 2016), although this may not be its only function. The *Drosophila fork head* gene was thought to regulate the transcription of other subordinate genes (Weigel et al., 1989), although the diversity of FOX domain proteins is extensive. The FOXA protein, for example, is a histone H1 mimic (Clark et al., 1993) and binds to nucleosome or nucleosome-free DNA, making it a pioneer transcription factor. It is unclear what the amino acids in the FOX domain that are unique to FOXG1 might do to alter its interaction with the genome. *FOXG1* is often described as a repressor (Tan et al., 2003; Yao et al., 2001), but there are insufficient data to rule out other transcriptional effects. We suggest remaining open to the possibilities of multiple other effects for *FOXG1*, both inside and outside the nucleus, as has been reported (Pancrazi et al., 2015). In our study, which did not investigate the molecular effects of *FOXG1*, we detected both a high- and a low-molecular-weight band in electrophoresis gels, suggesting that the fragment without the FOX domain may have non-DNA-binding functions (Hanashima et al., 2002).

FOXG1 has been implicated in both cell-proliferation and patterning defects. Patterning refers to cell signaling cues that dictate which type of cell a progenitor cell may become with respect to anterior-posterior and dorsal-ventral axes. In transgenic mouse studies, complete loss of *Foxg1* leads to the loss of the ventral telencephalon, which could be due to the absence of *Foxg1*-mediated patterning. For example, *Foxg1* may be needed to make cells competent to receive ventral-floor-plate morphogens such as Shh to allow ventralization (Huang et al., 2007; Huh et al., 1999). Alternatively, the expression level of *Foxg1* may determine the extent of blockade of dorsal-roof-plate morphogens such as WNT or BMP (Dou et al., 2000; Seoane et al., 2004), which are required for dorsalization (Lee and Jessell, 1999). This dosage effect of *Foxg1* might occur due to decreased association with the BMP antagonist *Foxh1* (Dou et al., 2000). In human cells, loss of *FOXG1* may allow for increased dorsalization of floor-plate structures due to increased competence of cells to dorsalize. While our work did not evaluate patterning effects of *FOXG1*, we cannot rule out that *in vitro* cell models lead to proliferation deficits as observed here due to altered cell response to exogenously added or endogenously produced morphogens. Proliferation deficits would then be a function of a different cell state, rather than a direct effect of *FOXG1* dose.

These data support a disease model of *FOXG1* syndrome in which *FOXG1* dose reduces the available number of forebrain NPCs in the developing brain (Ernst, 2016), possibly leading to primary microcephaly. These results are consistent with mouse transgenic studies showing significant loss of telencephalic progenitors (Hanashima et al., 2002; Hardcastle and Papalopulu, 2000; Xuan et al., 1995), although we could not distinguish between ventral and dorsal telencephalic cells in our model.

EXPERIMENTAL PROCEDURES

Subjects and cell lines

Case A and her biological mother (control A) were recruited at the Douglas Hospital Research Institute, where both individuals provided a urine sample for isolation of renal epithelial (RE) cells. Case A presented with severe motor impairments and intellectual disability. Genetic reports provided by the family indicated that she had a 14q12 heterozygous deletion approximately 4 Mb in length at position g.26,874,551–30,097,840 (NCBI Build GRCh37/hg19), deleting *FOXG1*. Case B and control B (biological mother) fibroblasts were acquired from the Coriell Institute (GM27244 and GM27246, respectively). Case B has a heterozygous variant in *FOXG1* c.256dup (p.Gln86Profs*35) leading to a frameshift in the coding sequence. Last, case C fibroblasts were acquired from Coriell (GM27190); the individual displayed epilepsy, hypotonia, and global developmental delay, among other symptoms. Whole-exome sequencing reported a nonsense mutation in *FOXG1* c.924G>A (p.W308X), leading to a premature truncation of the protein. As no familial control was available, we elected to use a non-related control line matched closely for sex and age (control C). All lines were obtained in adherence with ethical research principles and under protocols approved by the local institutional review board. Further details of all controls and cases can be found in Table S1. All *FOXG1* mutations were confirmed through PCR and Sanger sequencing using primers designed to target reported mutations. Further details on primers used can be found in Table S2.

Quality control of iPSCs

All iPSCs were rigorously assessed for contamination, pluripotency, and genomic integrity using several assays. All cells were tested for mycoplasma contamination (EZ-PCR Mycoplasma test kit, Biological Industries). Pluripotency was assessed by immunostaining with surface and nuclear pluripotency markers (Figure S2), and spontaneous 7-day embryoid body (EB) differentiation confirmed the capacity to form the three germ layers. All cases and edited lines were also assessed for large chromosomal aberrations (deletions,

break points) using a tiled sequencing array with probes biased toward 5,000–6,000 genes that may affect neurodevelopment. *De novo* CNVs >1 Mb were not observed in any lines (other than the known deletion in case A) in any of the probed genes.

Genetic engineering

A double nickase CRISPR-Cas9 gene-editing system with gRNA targeting intergenic FOXG1 was used to generate KO lines. One milligram of gRNA construct was added per transfection reaction, and transfection was carried out simultaneously with iPSC reprogramming to ensure clonality, as previously described (Bell et al., 2017). After transfection, cells were selected for puromycin resistance allowing for cell expansion from a single edited fibroblast or RE cell. Potentially edited colonies were expanded and stored as cell lines, after which DNA was extracted and Sanger sequenced at Genome Quebec. Additional data regarding CRISPR design, including the regions of *FOXG1* targeted and gRNA sequences, are found in Table S3. Protocols for gene editing of isogenic repair and inducible FOXG1 lines are detailed in the supplemental experimental procedures.

Quantitative PCR

Total DNA from control A and case A was assessed using qPCR to validate total DNA content in the reported ~4-Mb deletion in chromosome 14. The reactions were performed in a total volume of 20 μL on a 384-well plate using a QuantStudio 6 (Thermo Fisher) PCR machine. For each well, the qPCR mix included 5 μL of Luna Universal qPCR Master Mix (NEB), 0.5 μL of forward primer, 0.5 μL of reverse primer, 2 μL of H_2O, and 2 μL of cDNA, totaling 10 μL. Expression levels were given as a ratio between the relative quantities of the gene of interest and the endogenous control. β-actin was used as an internal control for normalization. The normalized expression levels were then compared between cell lines using ANOVA with a *post hoc* t test. Further details on the primers used for qPCR can be found in Table S2.

Western blotting

Cells were lysed with RIPA buffer (Sigma) supplemented with SIGMAFAST protease inhibitor tablets (Millipore-Sigma). Protein concentrations were determined using a Pierce BCA protein assay kit (Thermo Fisher). Approximately 15 μg of protein was loaded per well in Mini-PROTEAN TGX Stain-Free precast gels (Bio-Rad). Gels were run at 150 V for approximately 75 min, and then transferred to a nitrocellulose membrane using a Trans-Blot Turbo transfer system (Bio-Rad). Membranes were blocked in 4% non-fat milk dissolved in TBS-T buffer (Tris-buffered saline-Triton X; Sigma-Aldrich) for 20 min and then incubated with primary antibodies overnight at 4°C with shaking. Blots were washed three times in TBS-T for 5 min and then incubated with appropriate mouse or rabbit secondary antibodies for 1 h at room temperature. Blots were washed a further three times in TBS-T for 5 min and then imaged using a ChemiDoc XRS+ System (Bio-Rad). Blots were imaged and analyzed using ImageLab (Bio-Rad) software. Further details on the antibodies used can be found in Table S4.

Immunocytochemistry

Cells were plated on glass coverslips coated with Matrigel. Once cells were ready for immunofluorescence they were washed with phosphate-buffered saline (PBS) and fixed with 4% paraformaldehyde (Sigma-Aldrich) for 15 min. Samples were permeabilized with 0.5% TX-100 (Sigma-Aldrich) in 0.5% PBS-BSA for 15 min and then blocked in 0.5% PBS-BSA for an additional 15 min. Primary antibodies were added in appropriate dilutions in 0.5% PBS-BSA and added to samples for 30 min. Samples were washed, then 0.5% PBS-BSA containing an appropriate dilution of secondary antibody was added to the samples and incubated for 30 min in the dark. Samples were washed with 0.5% PBS-BSA and visualized on an Apotome fluorescence microscope (Zeiss). Further details on the antibodies used can be found in Table S5.

Data acquisition from immunofluorescence images

Images were taken on the Apotome fluorescence microscope (Zeiss) and quantification of immunofluorescence images was done using ImageJ 1.53.

BrdU fluorescence intensity

Merged images were split according to fluorescence channel (DAPI, blue; BrdU, green). Images were converted to an 8-bit mode allowing pixel values in a range between 0 and 255. A threshold was set for each channel to discriminate specific signal intensities from the background. The threshold was determined according to the condition presenting the highest signal-to-noise ratio. In the y axis of Figures 3B, 4D, 6C, and 7C, normalized BrdU intensity is defined as the integrated density (the product of area and mean gray value calculated in ImageJ) divided by the number of cells (DAPI-stained nuclei) counted. BrdU fluorescence intensity was normalized by the number of DAPI-positive pixels to minimize biases generated by differences in cell number between acquisition fields. Quantifications between groups were compared using t tests.

Counting primary cilia

Merged images were split according to fluorescence channel (DAPI, blue; cilia, red) using ImageJ. ARL13B (red) images were converted to binary, and the "analyze particles" function was used to count primary cilia. When cilia were stained for ARL13B (red), bright red dots/lines were counted as cilia. For each image, the proportion of ciliated nuclei was calculated. Nuclei (DAPI) were counted manually using the multi-point tool in ImageJ.

Statistical analyses

Error bars in plots represent the standard error of the mean (SEM). The t tests were based on two-tailed Student t tests. Statistical analyses and graphical outputs were generated using ggplot2 for R version 4.0.2. Statistical output and n are reported at all places data are reported.

Additional methods

Detailed information on Sanger sequencing, DNA extraction, FACS, and genetic engineering can be found in the supplemental experimental procedures.

SUPPLEMENTAL INFORMATION

Supplemental information can be found online at https://doi.org/10.1016/j.stemcr.2022.01.010.

AUTHOR CONTRIBUTIONS

C.E. and N.C.H. conceived the study and planned experiments. N.C.H., H.P., H.W., Y.Z., and X.Z. generated primary cell culture data. N.C.H. and V.Y. performed FACS analyses. N.C.H. and J.K. performed statistical analyses. N.C.H., H.P., H.W., V.S., G.M., and C.R.S. grew and collected patient somatic cells. X.Z., M.J., S.A., A.N., V.M., and L.A. validated antibodies for immunocytochemistry and western blot. A.S., G.T., E.A.F., T.M.D., and C.E. provided reagents and support. N.C.H. and C.E. wrote the manuscript.

CONFLICTS OF INTEREST

The authors declare no competing interests.

ACKNOWLEDGMENTS

We acknowledge funding by the FRQS doctoral program (N.C.H., V.M.), Indonesian Endowment Fund for Education PhD award (M.J.), CONACYT (Mexico) (L.A.), Canada Research Chairs program (C.E.), and a CIHR grant (C.E.). T.M.D. and E.A.F. received funding to support this project through the Alain and Sandra Bouchard Foundation for Intellectual Disabilities and the McGill Healthy Brains for Healthy Lives (HBHL) initiative. T.M.D. is further supported by the Mowafaghian Foundation and the Chamandy Foundation. E.A.F. is supported by a Foundation grant from the CIHR (FDN-154301) and a Canada Research Chair (Tier 1). We also acknowledge the services of the Molecular and Cellular Microscopy Platform (MCMP) and Melina Jaramillo Garcia at the Douglas Hospital Research Center for their kind assistance with imaging experiments.

Received: May 20, 2021
Revised: January 12, 2022
Accepted: January 13, 2022
Published: February 10, 2022

REFERENCES

Ardhanareeswaran, K., Mariani, J., Coppola, G., Abyzov, A., and Vaccarino, F.M. (2017). Human induced pluripotent stem cells for modelling neurodevelopmental disorders. Nat. Rev. Neurol. *13*, 265–278. https://doi.org/10.1038/nrneurol.2017.45.

Ariani, F., Hayek, G., Rondinella, D., Artuso, R., Mencarelli, M.A., Spanhol-Rosseto, A., Pollazzon, M., Buoni, S., Spiga, O., Ricciardi, S., et al. (2008). FOXG1 is responsible for the congenital variant of Rett syndrome. Am. J. Hum. Genet. *83*, 89–93. https://doi.org/10.1016/j.ajhg.2008.05.015.

Bell, S., Peng, H., Crapper, L., Kolobova, I., Maussion, G., Vasuta, C., Yerko, V., Wong, T.P., and Ernst, C. (2017). A rapid pipeline to model rare neurodevelopmental disorders with simultaneous CRISPR/Cas9 gene editing. Stem Cells Transl. Med. *6*, 886–896. https://doi.org/10.1002/sctm.16-0158.

Bell, S., Hettige, N.C., Silveira, H., Peng, H., Wu, H., Jefri, M., Antonyan, L., Zhang, Y., Zhang, X., and Ernst, C. (2019). Differentiation of human induced pluripotent stem cells (iPSCs) into an effective model of forebrain neural progenitor cells and mature neurons. Bio Protoc. *9*, e3188. https://doi.org/10.21769/BioProtoc.3188.

Cargnin, F., Kwon, J.S., Katzman, S., Chen, B., Lee, J.W., and Lee, S.K. (2018). FOXG1 orchestrates neocortical organization and cortico-cortical connections. Neuron *100*, 1083–1096 e5. https://doi.org/10.1016/j.neuron.2018.10.016.

Caviness, V.S., Jr., Takahashi, T., and Nowakowski, R.S. (1995). Numbers, time and neocortical neuronogenesis: a general developmental and evolutionary model. Trends Neurosci. *18*, 379–383. https://doi.org/10.1016/0166-2236(95)93933-o.

Chambers, S.M., Fasano, C.A., Papapetrou, E.P., Tomishima, M., Sadelain, M., and Studer, L. (2009). Highly efficient neural conversion of human ES and iPS cells by dual inhibition of SMAD signaling. Nat. Biotechnol. *27*, 275–280. https://doi.org/10.1038/nbt.1529.

Chen, J., Wu, X., Xing, Z., Ma, C., Xiong, W., Zhu, X., and He, X. (2018). FOXG1 expression is elevated in glioma and inhibits glioma cell apoptosis. J. Cancer *9*, 778–783. https://doi.org/10.7150/jca.22282.

Clark, K.L., Halay, E.D., Lai, E., and Burley, S.K. (1993). Co-crystal structure of the HNF-3/fork head DNA-recognition motif resembles histone H5. Nature *364*, 412–420. https://doi.org/10.1038/364412a0.

Cloughesy, T.F., Cavenee, W.K., and Mischel, P.S. (2014). Glioblastoma: from molecular pathology to targeted treatment. Annu. Rev. Pathol. *9*, 1–25. https://doi.org/10.1146/annurev-pathol-011110-130324.

Dastidar, S.G., Landrieu, P.M., and D'Mello, S.R. (2011). FoxG1 promotes the survival of postmitotic neurons. J. Neurosci. *31*, 402–413. https://doi.org/10.1523/JNEUROSCI.2897-10.2011.

Dou, C., Lee, J., Liu, B., Liu, F., Massague, J., Xuan, S., and Lai, E. (2000). BF-1 interferes with transforming growth factor beta signaling by associating with Smad partners. Mol. Cell. Biol. *20*, 6201–6211. https://doi.org/10.1128/mcb.20.17.6201-6211.2000.

Egger, B., Gold, K.S., and Brand, A.H. (2011). Regulating the balance between symmetric and asymmetric stem cell division in the developing brain. Fly (Austin) *5*, 237–241. https://doi.org/10.4161/fly.5.3.15640.

Ernst, C. (2016). Proliferation and differentiation deficits are a major convergence point for neurodevelopmental disorders. Trends Neurosci. *39*, 290–299. https://doi.org/10.1016/j.tins.2016.03.001.

Foley, A.C., Skromne, I., and Stern, C.D. (2000). Reconciling different models of forebrain induction and patterning: a dual role for the hypoblast. Development *127*, 3839–3854.

Golson, M.L., and Kaestner, K.H. (2016). Fox transcription factors: from development to disease. Development *143*, 4558–4570. https://doi.org/10.1242/dev.112672.

Guemez-Gamboa, A., Coufal, N.G., and Gleeson, J.G. (2014). Primary cilia in the developing and mature brain. Neuron *82*, 511–521. https://doi.org/10.1016/j.neuron.2014.04.024.

Hanashima, C., Shen, L., Li, S.C., and Lai, E. (2002). Brain factor-1 controls the proliferation and differentiation of neocortical progenitor cells through independent mechanisms. J. Neurosci. *22*, 6526–6536.

Hanashima, C., Li, S.C., Shen, L., Lai, E., and Fishell, G. (2004). Foxg1 suppresses early cortical cell fate. Science *303*, 56–59. https://doi.org/10.1126/science.1090674.

Hanzlik, E., and Gigante, J. (2017). Microcephaly. Children (Basel) *4*, 47. https://doi.org/10.3390/children4060047.

Hardcastle, Z., and Papalopulu, N. (2000). Distinct effects of XBF-1 in regulating the cell cycle inhibitor p27(XIC1) and imparting a neural fate. Development *127*, 1303–1314.

Hettige, N.C., and Ernst, C. (2019). FOXG1 dose in brain development. Front. Pediatr. *7*, 482. https://doi.org/10.3389/fped.2019.00482.

Homem, C.C., Repic, M., and Knoblich, J.A. (2015). Proliferation control in neural stem and progenitor cells. Nat. Rev. Neurosci. *16*, 647–659. https://doi.org/10.1038/nrn4021.

Huang, X., Litingtung, Y., and Chiang, C. (2007). Ectopic sonic hedgehog signaling impairs telencephalic dorsal midline development: implication for human holoprosencephaly. Hum. Mol. Genet. *16*, 1454–1468. https://doi.org/10.1093/hmg/ddm096.

Huh, S., Hatini, V., Marcus, R.C., Li, S.C., and Lai, E. (1999). Dorsal-ventral patterning defects in the eye of BF-1-deficient mice associated with a restricted loss of shh expression. Dev. Biol. *211*, 53–63. https://doi.org/10.1006/dbio.1999.9303.

Kohwi, M., and Doe, C.Q. (2013). Temporal fate specification and neural progenitor competence during development. Nat. Rev. Neurosci. *14*, 823–838. https://doi.org/10.1038/nrn3618.

Lathia, J.D., Mack, S.C., Mulkearns-Hubert, E.E., Valentim, C.L., and Rich, J.N. (2015). Cancer stem cells in glioblastoma. Genes Dev. *29*, 1203–1217. https://doi.org/10.1101/gad.261982.115.

Lee, K.J., and Jessell, T.M. (1999). The specification of dorsal cell fates in the vertebrate central nervous system. Annu. Rev. Neurosci. *22*, 261–294. https://doi.org/10.1146/annurev.neuro.22.1.261.

Li, J., and Vogt, P.K. (1993). The retroviral oncogene qin belongs to the transcription factor family that includes the homeotic gene fork head. Proc. Natl. Acad. Sci. U S A *90*, 4490–4494. https://doi.org/10.1073/pnas.90.10.4490.

Liu, S., Trupiano, M.X., Simon, J., Guo, J., and Anton, E.S. (2021). The essential role of primary cilia in cerebral cortical development and disorders. Curr. Top. Dev. Biol. *142*, 99–146. https://doi.org/10.1016/bs.ctdb.2020.11.003.

Murphy, D.B., Wiese, S., Burfeind, P., Schmundt, D., Mattei, M.G., Schulz-Schaeffer, W., and Thies, U. (1994). Human brain factor 1, a new member of the fork head gene family. Genomics *21*, 551–557. https://doi.org/10.1006/geno.1994.1313.

Nieuwkoop, P.D. (1947). Investigations on the regional determination of the central nervous system. J. Exp. Biol. *24*, 145–183.

Pancrazi, L., Di Benedetto, G., Colombaioni, L., Della Sala, G., Testa, G., Olimpico, F., Reyes, A., Zeviani, M., Pozzan, T., and Costa, M. (2015). Foxg1 localizes to mitochondria and coordinates cell differentiation and bioenergetics. Proc. Natl. Acad. Sci. U S A *112*, 13910–13915. https://doi.org/10.1073/pnas.1515190112.

Patriarchi, T., Amabile, S., Frullanti, E., Landucci, E., Lo Rizzo, C., Ariani, F., Costa, M., Olimpico, F., Hell, J.W., Vaccarino, F.M., et al. (2016). Imbalance of excitatory/inhibitory synaptic protein expression in iPSC-derived neurons from FOXG1(+/-) patients and in foxg1(+/-) mice. Eur. J. Hum. Genet. *24*, 871–880. https://doi.org/10.1038/ejhg.2015.216.

Pugacheva, E.N., Jablonski, S.A., Hartman, T.R., Henske, E.P., and Golemis, E.A. (2007). HEF1-dependent Aurora A activation induces disassembly of the primary cilium. Cell *129*, 1351–1363. https://doi.org/10.1016/j.cell.2007.04.035.

Rakic, P. (2006). A century of progress in corticoneurogenesis: from silver impregnation to genetic engineering. Cereb. Cortex *16* (*Suppl 1*). i3–17. https://doi.org/10.1093/cercor/bhk036.

Rakic, P., and Caviness, V.S., Jr. (1995). Cortical development: view from neurological mutants two decades later. Neuron *14*, 1101–1104. https://doi.org/10.1016/0896-6273(95)90258-9.

Sanchez, I., and Dynlacht, B.D. (2016). Cilium assembly and disassembly. Nat. Cell Biol. *18*, 711–717. https://doi.org/10.1038/ncb3370.

Seoane, J., Le, H.V., Shen, L., Anderson, S.A., and Massague, J. (2004). Integration of Smad and forkhead pathways in the control of neuroepithelial and glioblastoma cell proliferation. Cell *117*, 211–223. https://doi.org/10.1016/s0092-8674(04)00298-3.

Szymczak, A.L., and Vignali, D.A. (2005). Development of 2A peptide-based strategies in the design of multicistronic vectors. Expert Opin. Biol. Ther. *5*, 627–638. https://doi.org/10.1517/14712598.5.5.627.

Takahashi, K., Tanabe, K., Ohnuki, M., Narita, M., Ichisaka, T., Tomoda, K., and Yamanaka, S. (2007). Induction of pluripotent stem cells from adult human fibroblasts by defined factors. Cell *131*, 861–872. https://doi.org/10.1016/j.cell.2007.11.019.

Tan, K., Shaw, A.L., Madsen, B., Jensen, K., Taylor-Papadimitriou, J., and Freemont, P.S. (2003). Human PLU-1 Has transcriptional repression properties and interacts with the developmental transcription factors BF-1 and PAX9. J. Biol. Chem. *278*, 20507–20513. https://doi.org/10.1074/jbc.M301994200.

Tao, W., and Lai, E. (1992). Telencephalon-restricted expression of BF-1, a new member of the HNF-3/fork head gene family, in the developing rat brain. Neuron *8*, 957–966. https://doi.org/10.1016/0896-6273(92)90210-5.

Verginelli, F., Perin, A., Dali, R., Fung, K.H., Lo, R., Longatti, P., Guiot, M.C., Del Maestro, R.F., Rossi, S., di Porzio, U., et al. (2013). Transcription factors FOXG1 and Groucho/TLE promote glioblastoma growth. Nat. Commun. *4*, 2956. https://doi.org/10.1038/ncomms3956.

Waters, A.M., and Beales, P.L. (2011). Ciliopathies: an expanding disease spectrum. Pediatr. Nephrol. *26*, 1039–1056. https://doi.org/10.1007/s00467-010-1731-7.

Weigel, D., Jurgens, G., Kuttner, F., Seifert, E., and Jackle, H. (1989). The homeotic gene fork head encodes a nuclear protein and is expressed in the terminal regions of the Drosophila embryo. Cell *57*, 645–658. https://doi.org/10.1016/0092-8674(89)90133-5.

Xuan, S., Baptista, C.A., Balas, G., Tao, W., Soares, V.C., and Lai, E. (1995). Winged helix transcription factor BF-1 is essential for the development of the cerebral hemispheres. Neuron *14*, 1141–1152. https://doi.org/10.1016/0896-6273(95)90262-7.

Yao, J., Lai, E., and Stifani, S. (2001). The winged-helix protein brain factor 1 interacts with groucho and hes proteins to repress transcription. Mol. Cell. Biol. *21*, 1962–1972. https://doi.org/10.1128/MCB.21.6.1962-1972.2001.

Zhu, W., Zhang, B., Li, M., Mo, F., Mi, T., Wu, Y., Teng, Z., Zhou, Q., Li, W., and Hu, B. (2019). Precisely controlling endogenous protein dosage in hPSCs and derivatives to model FOXG1 syndrome. Nat. Commun. *10*, 928. https://doi.org/10.1038/s41467-019-08841-7.